Enhancement of Triple Negative Breast Cancer Virotherapy via Alkylating Agent-Induced Autophagy

Roxana Gonzalez-Ramos [1, 2], Akiko Chiba [3], Lacey McNally [4], Kelly M. McMasters[1, 2], and Jorge G. Gomez-Gutierrez [1,2]

[1]The Hiram C. Polk MD Department of Surgery, [2]James Graham Brown Cancer Center, University of Louisville, Louisville, KY, 40202.

[3] Department of Surgery, [4] Department of Cancer Biology at Wake Forest Comprehensive Cancer Center, Wake Forest University, Winston-Salem, NC.

Introduction

Oncolytic virotherapy has made significant progress in recent years, however, widespread approval of virotherapeutics is still limited. Primarily, this is due to the fact that currently available virotherapeutics are mostly tested in monotherapeutic clinical trials exclusively (i.e, not in combination with other therapies) and so far have achieved only small and often clinically insignificant responses. For this reason, combination strategies of virotherapy with highly genotoxic regimens, such as chemotherapy, are of major interest.

Triple negative breast cancer (TNBC) occurs in about 10-20% of diagnosed breast cancers and is more likely to affect younger women, African Americans, Hispanics and/or those with BRCA 1 gene mutation, in comparison with estrogen receptor positive breast cancer, TNBC can be more aggressive and difficult to treat. TNBC does not respond to hormonal therapy (e.g. Tamoxifen), however it could respond to conventional chemotherapy.

We hypothesize that Alkylating agent induced-autophagy can increase oncolytic virus replication in TNBC cells. In this study, the alkylating agent temozolomide (TMZ) was combined with a oncolytic adenovirus (OAd) in which the capsid was genetically labeled with the fluorescent reporter of the “mFruit” family with far-red emission spectra, mCherry. The red florescent “mCherry” reporter gene was fusioned to viral capsid protein IX.

It was found that TMZ increased AdmCherry-replication and oncolysis TNBC cells. The increased OAdmCherry potency was associated with an increase on E1A expression and virus production. The combined therapy of AdmCherry with TMZ resulted in a greater killing effect than either agent alone. This increased killing effect was associated with apoptosis induction and accumulation of the autophagy marker LC3-II.

Results

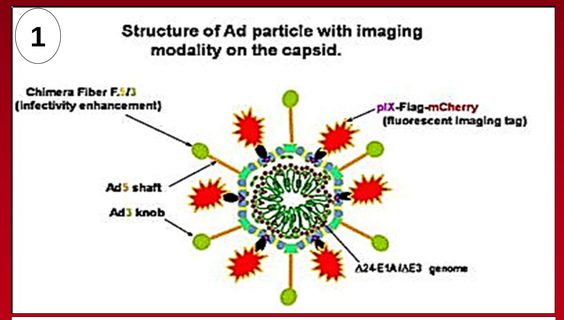

Fig. 1 The capsid OAdmCherry was genetically labeled with the fluorescent reporter of the “mFruit” family with far-red emission spectra, mCherry. The red florescent “mCherry” reporter gene was fusioned to viral capsid protein IX.

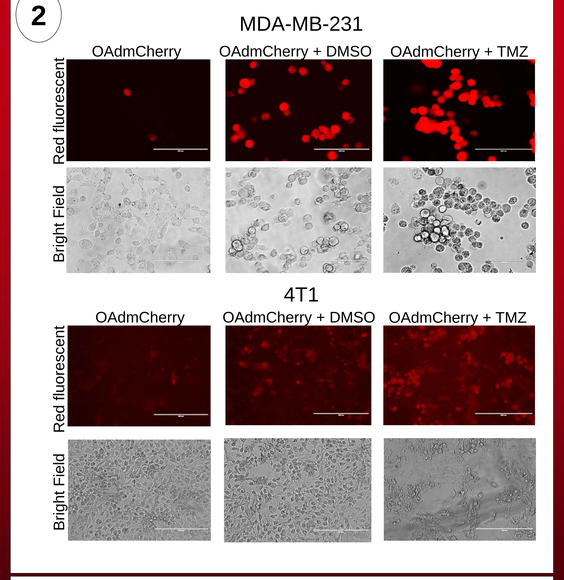

Fig. 2. Temozolomide increases Oad replication and spread in both human and murine TNBC cells. MDA-MB-231 and 4T1 cells were infected with OAdmCherry followed by either veichle contro DMSO or TMZ, 72 h post treatment mCherry expression was visualized by florescent microscope.

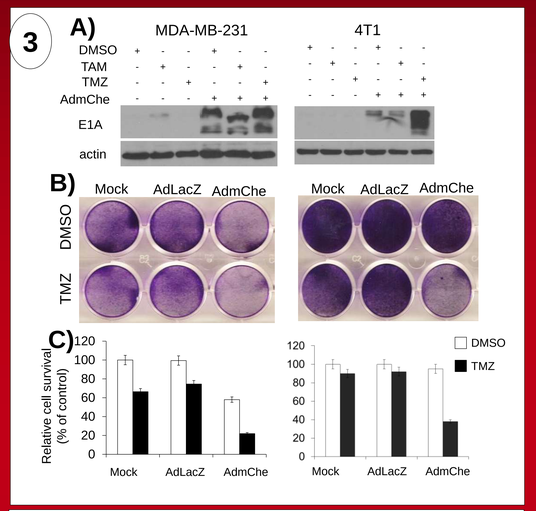

Fig. 3 TMZ upregulate Ad E1A expression and increases cytopathic effect. A) Expression of Ad E1A and actin as loading control. **B)** Crystal violet staining. **C)** Cell viability was calculated by measuring the absorbance of solubilized dye at 590 nm. Each point represents the mean of three independent experiments ± standard deviation (SD; *bars*).

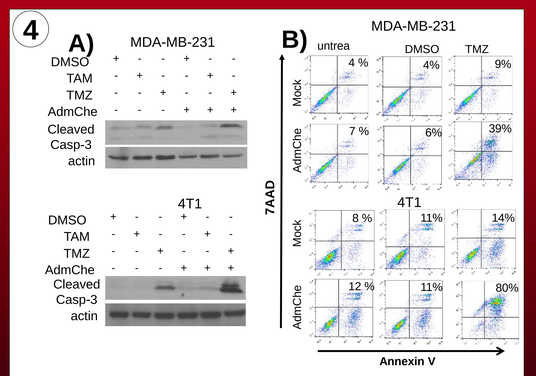

Fig. 4 Evaluation of apoptosis induction by the combined therapy in human and murine TNBC cells. A) Capase-3 activation. B) Annexin V staining.

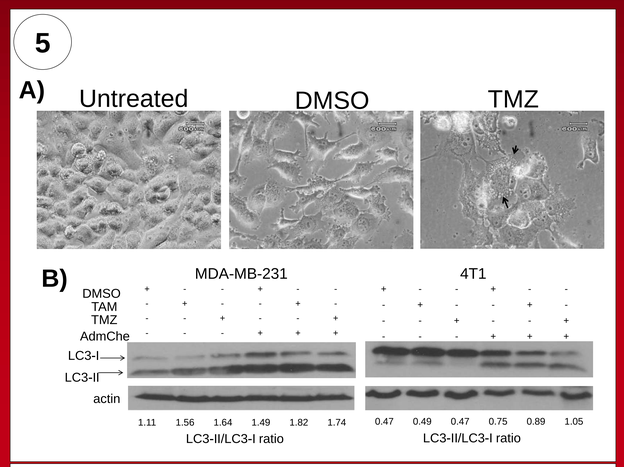

Fig. 5 Effect of combined therapy on LC3 autophagy marker expression in TNBC cells. A) TNBC displaying vesiculated cytoplasm after TMZ treatment**. B)** Tow forms of LC3 were detected, LC3-I and LC3-II, an increase on LC3-II and decrease on LC3-I indicates autophagy activation.

Conclusions

This study, provides the experimental evidence showing that TMZ can be used to enhance TNBC virotherapy which may represent an alternative approach to destroy TNBC tumors in patients with resistance to chemotherapy. Most importantly, TMZ enhanced OAd mediated-oncolysis in the murine 4T1 cells that represent the stage IV of human BC and triple negative breast cancer were efficiently killed by the combined therapy of oncolytic adenovirus with TMZ. In addition, these chemovirotherapies may allow for use of less-toxic doses to achieve therapeutic efficacy and prime immune system to reduce the chances of cancer recurrences.

Acknowledgements

Research supported by the University of Louisville Cancer Education Program grant R25-CA-134283 from the National Cancer Institute.

The Effect of PFKFB4 Inhibition on the Cell Cycle Progression of Medulloblastoma Cells

Meranda Hinds[1], Brandi Radde, B.S.[1], Nadiia Lypova, Ph.D[1], Sucheta Telang, MBBS[1,2]
Departments of Medicine[1] and Pediatrics[2]
University of Louisville School of Medicine

♦ Introduction

Many cancer cell types demonstrate increased glycolytic metabolism to support the needs of their rapid proliferation. The conversion of fructose-6-phosphate (F6P) to fructose-1,6-bisphosphate (F16BP) through the enzymatic activity of phosphofructokinase-1 (PFK1) is an important rate-limiting step in the glycolytic pathway. High levels of ATP and citrate provide negative feedback at this step, inhibiting the advancement along the glucose metabolic pathway when a cell has sufficient energy stores. Fructose-2,6-bisphosphate (F26BP) has been found to be a powerful allosteric activator of PFK1 that is capable of overriding the negative feedback inhibition provided by ATP and citrate, thus stimulating the conversion of F6P to F16BP and propagating this metabolic pathway regardless of a cancer cell's energy needs. F26BP is the product of the 6-phosphofructokinase/fructose-2,6-bisphosphatase family of enzymes (PFKFB1-4), which interconvert F6P and F26BP. We have previously found that medulloblastoma cells express high levels of the PFKFB4 isoform and that silencing PFKFB4 expression decreases F26BP production and proliferation in these cells. We hypothesized that the decrease in proliferation may be due to an arrest in cell cycle progression.

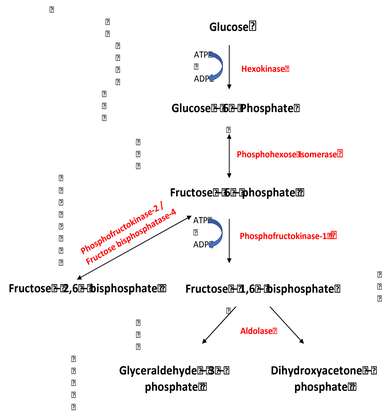

Figure 1. Schematic depicting the initial steps in the glycolysis metabolic pathway, including the product, fructose-2,6-bisphosphate produced through the enzymatic activity of PFKFB1-4.

In order to examine this hypothesis, we silenced PFKFB4 expression using small interfering RNA (siRNA) and examined the effect of silencing PFKFB4 on cell cycle progression in Daoy medulloblastoma cells using flow cytometry. We then compared this effect with the effect of a small molecule inhibitor of PFKFB4 (FB4i) on the Daoy cells.

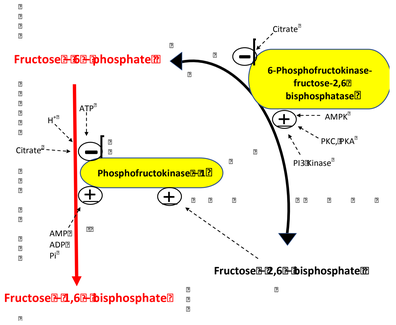

Figure 2. Schematic detailing the role of PFKFB1-4 in glycolysis and the feedback loops used to regulate it and PFK-1.

♦ Materials and Methods

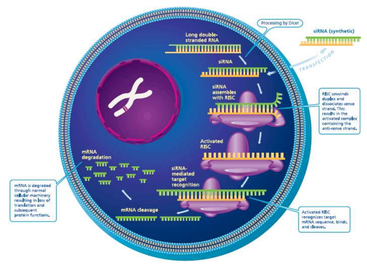

Figure 3. Diagram of siRNA and the mechanism it uses to degrade target mRNA sequences and silence genes. (*http://www.sigmaaldrich.com/technical-documents*)

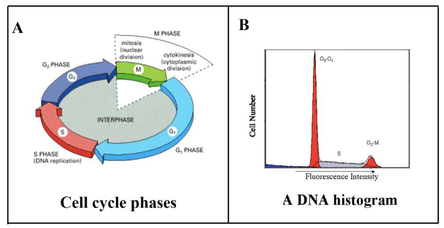

Figure 4. Diagram showing the cell cycle and the corresponding peaks on a flow cytometry histogram. (*Ashraf Tabll and Hisham Ismail, InTech, 2011, DOI: 10.5772/19384*)

siRNA treatment: Daoy cells plated in 6 well plates were transfected with siRNA targeting PFKFB4 or a nonsense siRNA (20 nM) using the transfection reagent Lipofectamine RNAiMax and incubated for 72 hours under either hypoxic (1% oxygen) or normoxic (21% oxygen) conditions and then harvested for Western blot and cell cycle analyses.

Inhibitor treatment: Daoy cells plated in 6 well plates were treated with a small molecule inhibitor of PFKFB4 (FB4i) for 72 hours and then harvested for cell cycle analyses.

Cell cycle analyses: Following harvest, cells were washed with cold PBS and fixed in 70% ethanol at 4°C for 30 minutes. Cells were then pelleted by centrifugation, resuspended in PBS containing propidium iodide and RNAse A, incubated at 37°C for 30 minutes and analyzed by flow cytometry. Data shown are representative of 2 experiments.

♦ Results

Western Blot Analysis of PFKFB4 knockdown under normoxic and hypoxic conditions

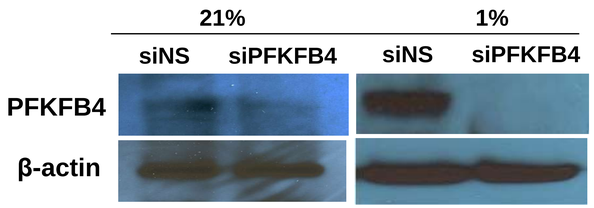

Distribution of cells in phases of the cell cycle following PFKFB4 knockdown in normoxia

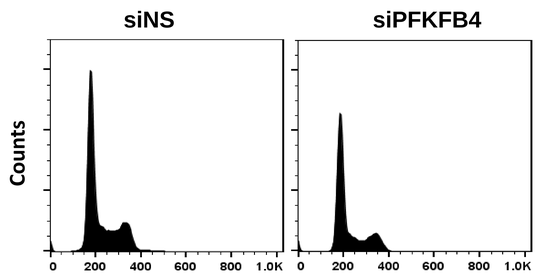

G1/G0: 47.2%
S: 20.5%
G2/M: 27.7%

G1/G0: 58.9%
S: 22.3%
G2/M: 16.3%

Distribution of cells in phases of the cell cycle following PFKFB4 inhibition in normoxia

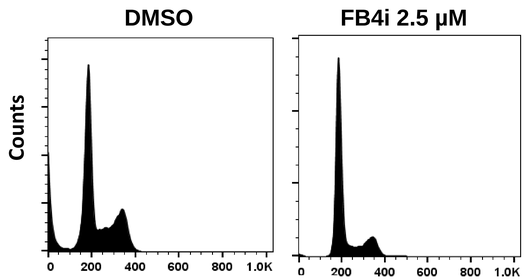

G1/G0: 49.6%
S: 26.5%
G2/M: 20.3%

G1/G0: 58.1%
S: 24.1%
G2/M: 26.9%

♦ Conclusion

Our data suggest that siRNA knockdown of PFKFB4 expression and inhibition of the activity of PFKFB4 with a small molecule inhibitor cause a similar G0/G1 arrest in Daoy medulloblastoma cells. Future studies will further examine the effects of small molecule inhibition of PFKFB4 on medulloblastoma. It is our hope that this study will enhance the future study of this bifunctional enzyme and the glycolytic pathway in medulloblastoma cells so that it can be determined if PFKFB4 inhibition may serve as a potential target in medulloblastoma.

♦ Future Directions

- Further study the effects of PFKFB4 small molecule inhibition in medulloblastoma.
- Examine the effects of PFKFB4 inhibition under hypoxia on cell cycle progression.
- Compare the effect of knocking down one of the other three isoforms of PFKFB (1-3) with the results from PFKFB4 knockdown

♦ Acknowledgements

Research funded by the National Cancer Institute grant R25 C-A134283 and the University of Louisville Cancer Education Program.

Effect of Expression of Constitutive Active Retinoblastoma Protein (Rb) on Glucose Metabolism
An Exercise in Experimental Troubleshooting

Joshua Julian, Lindsey Reynolds, and Brian Clem

James Graham Brown Cancer Center, Dept, of Biochemistry and Molecular Genetics, University of Louisville School of Medicine

Introduction

Investigation into the metabolism of cancer cells has implicated a potential role for the retinoblastoma protein (RB) tumor suppressor, which has been classically defined in controlling cell proliferation. When active, Rb binds to a family of transcription factors, termed E2Fs, that regulate a number of cellular processes. Since inactivation of Rb has been observed in most forms of cancer, it is plausible that loss of Rb function might alter glucose metabolism by regulating specific metabolic enzymes.

Objective and Hypothesis

We attempted to express a constitutively active form of RB (phosphorylation site mutated Rb or PSM-Rb) in HCT116 cells and monitor changes in glucose metabolism through both glucose uptake and glycolysis assays. We hypothesized that cells overexpressing PSM-Rb would show a decrease in glucose metabolism.

Methods

Cell Culture: HEK 293T cells were maintained in culture using DMEM supplemented with 10% FBS and gentamicin, and the HCT116 cells were grown in McCoy's medium with 10% FBS and gentamicin.

Cell Transfections: HCT116 cells were plated in 6-well culture dishes and transfected 24 hours later with pcDNA-PSM or empty vector for 4 hours. Transfection medium was replaced with complete medium and left for 48-hours until subsequent assays were performed. Transfection of GFP vector with pcDNA-PSM or the control vector was performed in HCT116 cells using the jetPRIME system. Expression of GFP was determined by fluorescent microscopy (EVOS)

Retrovirus production and viral infection: HEK 293T cells were transfected with pUMVC+PMRG retroviral packaging plasmids and the retroviral pQCXIH-PSM vector via the jetPRIME system. Viral supernatant was collected 48 hours later and used in varying amounts to infect HCT116 cells. Infected cells were compared to untreated samples 48 hours later.

Cell sorting: Flow cytometry (Molflo) was used to sort the GFP/PSM- and GFP/control-cotransfected cells collected in 1mL of medium. Glucose uptake assay was immediately performed on pelleted cells.

Western blotting: Protein lysates from transfected or retrovirus infected cells were separated by SDS-PAGE. Proteins were then transferred to PVDF membrane and probed for both PSM-Rb and actin expression.

Glucose uptake Assay: Glucose starved transfected/infected cells were incubated with 14C-2-deoxy-glucose. Cells were washed, lysed with SDS, and intracellular glucose was measured via scintillation counting normalized to protein content.

Glycolysis assay: Transfected/infected cells were incubated with 3H-glucose. 3H2O release into the media was then assessed by scintillation counting after equilibration with diH2O in evaporation chambers for 48-72 hours.

PSM-Rb

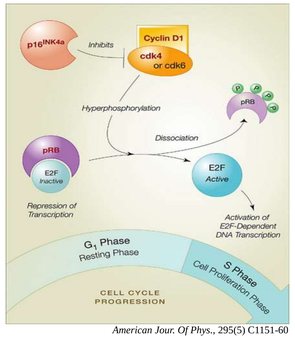

American Jour. Of Phys., 295(5) C1151-60

Figure 1: Schematic representation of Rb inactivation by phosphorylation and subsequent E2F function.

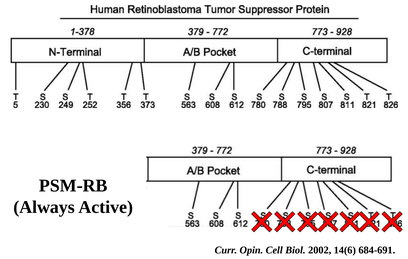

Curr. Opin. Cell Biol. 2002, 14(6) 684-691.

Figure 2: Schematic comparison of PSM-Rb to WT-Rb with sites of amino acid mutations to prevent phosphorylation.

PSM-Rb Transient Transfection

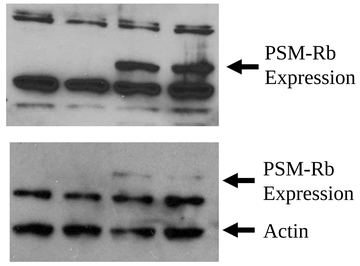

Figure 3: Western blot of PSM-Rb-transfected cells with actin loading control. (1-2) Ctrl cells (3-4) PSM transfected cells.

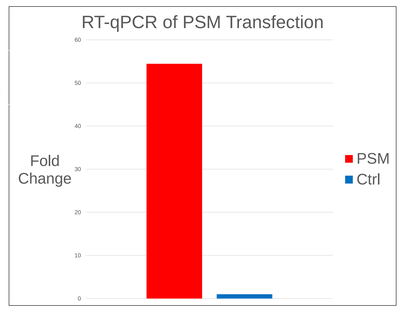

Figure 4: RT-qPCR data showing expression levels in transfected HCT116 cells.

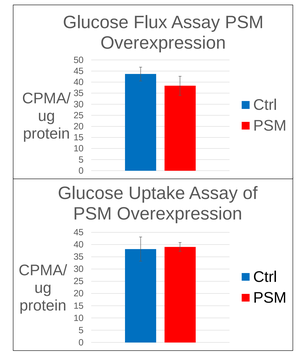

Figure 5: Glycolysis and glucose uptake assays on transfected HCT116 cells.

Retroviral PSM-Rb Infection

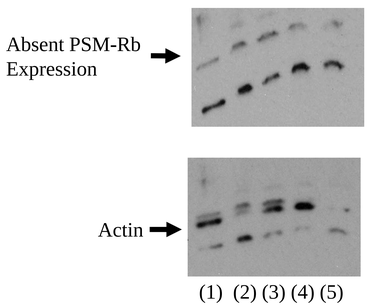

Figure 6: Western blot of retroviral PSM-Rb-infected HCT-116 cells with actin loading control. (1) PSM-infected cells (2) 1mL Ctrl (3-5) Ctrl

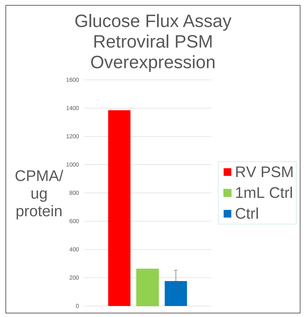

Figure 7: Glycolysis assay between infected cells and control.

GFP/PSM-Rb Cell Sorting

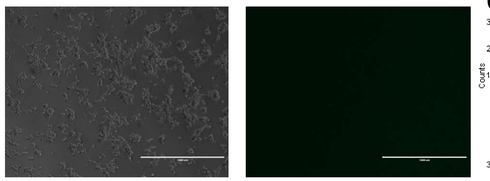

Figure 8: Imaging of control cells (without GFP)

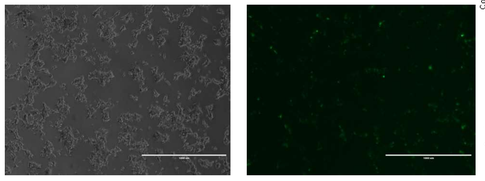

Figure 9: Imaging of GFP/PSM-Rb transfected cells

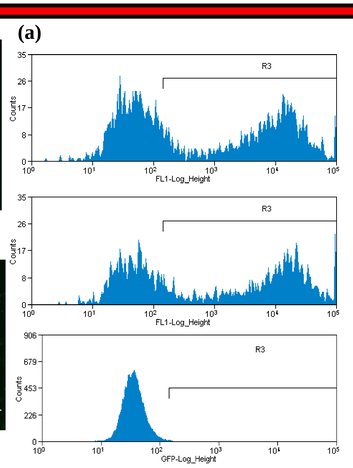

Figure 10: (a) Flow chart of GFP levels in and sorting of GFP/control and GFP/PSM cells, and sorting gate from control (top to bottom). (b) Glucose uptake assay on GFP-sorted HCT116 cells.

Conclusion/Future Direction

These preliminary results suggest a lack of direct metabolic influence by PSM-RB, but, there remains a need for optimization for PSM-Rb expression. This includes protein analysis by Western blotting to assess the expression of PSM in the GFP-sorted cells. In addition, the GFP and PSM pcDNA should also be encapsulated in the same vector to ensure any cell that expresses GFP will also express PSM. Finally, all the metabolic assays should be repeated on each of the methods as each assay was performed once per method. Further evaluation of the results found during this program will hopefully produce an optimized method of transfecting PSM-Rb so the investigation of the effects of constitutively RB can be elucidated.

Acknowledgements/Grant Support

R25 Program UofL CEP through James Graham Brown Cancer Center. NIH/NCI (R25-CA134283).

Mechanisms by which rapamycin protects from liver damage caused by VC metabolites in mice.

Austin M. Krueger[1], Anna L. Lang[1], Brenna R. Kaelin[1],and Juliane I. Beier[1]

[1] Department of Pharmacology and Toxicology, University of Louisville, Louisville, KY 40202, USA

ABSTRACT

Background: Vinyl chloride (VC) is a pervasive, organochlorine toxicant characterized by a colorless, mildly ordered gas at room temperature. The majority of the production of VC is used in the manufacturing of polyvinyl chloride (PVC). PVC is predominantly used in the production of a variety of plastic containing materials. VC has been known to cause liver damage at high occupational doses, although low exposure to VC is not yet fully understood.

Methods: C57BL/6J mice were administered chloroethanol (CE), a VC metabolite, then rapamycin one hour following the CE administration. 24-hours following the CE exposure, the mice were administered lipopolysaccharide (LPS), an inflammatory stimulus. The mice were then sacrificed 4 or 24 hours following LPS administration.

Results: It was found that the control mice were shown to exhibit normal liver morphology and function. Those administered with CE alone showed no liver pathology but an altered metabolic profile. LPS alone increased inflammatory damage. CE and LPS significantly enhanced inflammation, necrotic cell death, and significant glycogen depletion. The addition of rapamycin significantly dampened the inflammatory response of CE+LPS mice via mTOR inhibition and oxidative stress pathways.

Conclusions: This study shows that the upregulation of mTOR through CE exposure can contribute to liver injury. It was found that the presence of rapamycin may dampen the impact that CE+LPS has on liver damage, fat accumulation, and inflammation as well as measurable glycogen depletions. As seen with the addition of rapamycin, the mTOR pathway plays a significant role in VC metabolite induced liver damage and oxidative stress.

BACKGROUND

Vinyl chloride (VC) is a relevant chemical toxicant and an important occupational/environmental pollutant. It is released by industries or formed by the breakdown of other chlorinated chemicals, such as TCE and PCE (e.g., in landfills), and enters the air and drinking water supplies. For example, up to 1,000,000 individuals were exposed to VC-contaminated drinking water at the Camp Lejeune, NC Superfund site alone.[2] Recent studies by our group have shown that high occupational exposures to VC can cause toxicant-associated steatohepatitis (TASH).[2] However, most studies on the risk of VC exposure to human health have focused on the effect of VC alone (high doses) and not taken into consideration VC interactions (low doses) with risk-modifying factors. Numerous studies have now established that physiological/biochemical changes to liver that are pathologically inert can become hepatotoxic in response to a second agent. This '2-hit' paradigm has been best exemplified in non-alcoholic fatty liver diseases.[3] We propose that low-dose VC may also serve as a second hit with other risk modifying factors.

Data from our lab show that VC/VC metabolites alter cytokine production and cause mitochondrial dysfunction resulting in disruptions of hepatic carbohydrate and lipid metabolism. Another finding of that study was a strong activation of the mammalian target of rapamycin (mTOR).[6] Activation of mTOR plays a critical role between pathways that regulate the balance between cell survival, macromolecule synthesis, and inflammation in response to nutritional, growth, and stress signals. Our data support mTOR activation is critically involved in liver injury and damage caused by VC metabolites. Therefore, the goal of this study was to inhibit mTOR with rapamycin to determine its role in liver damage caused by VC metabolite exposure and elucidate mechanisms of pathogenesis.

This project's goal was to determine mechanisms by which mTOR inhibition protects against liver injury and oxidative stress in this mouse model. It is known that TERT protects Src inactivation,[8] further halting the impact on the Electron Transport Chain (ETC) and the production of Reactive Oxygen Species (ROS). The phosphorylation of Shp-1 is shown to increase the ability of DOK4's role in the activation of Src.[7] The phosphorylation Src leads to an increase in production from the ETC, however, the de-phosphorylation of Src uncouples the ETC causing an increase in the production of ROS.[7] Therefore, the purpose of this project was to investigate this TERT-Src-Shp pathway as a potential mechanism by which rapamycin protects against liver injury.

MATERIALS AND METHODS

Animals. Eight-week-old, male C57BL/6J mice were administered chloroethanol (CE), a VC metabolite, then rapamycin one hour following the CE administration. 24-hours following the CE exposure, the mice were administered lipopolysaccharide (LPS), an inflammatory metabolite. The mice were then sacrificed 4-hours following the LPS administration.

Immunoblots. Protein was extracted from hepatic tissue. 50 µg of total protein was loaded onto SDS–polyacrylamide gels followed by electrophoresis and Western blotted onto PVDF membranes. Antibodies were used at the dilutions recommended by the suppliers. Horseradish peroxidase-coupled secondary antibodies and chemiluminescence detection reagents were from Pierce (Rockford, IL, USA). The signals were detected employing Classic Blue™ autoradiography film BX (MIDSCI, St. Louis, MO) and a Molecular Imager ChemiDoc XRS System (Universal Hood II, Bio-Rad) were used. Densitometric quantitation was performed with UN-SCAN IT analysis software (Silk Scientific, Orem, UT).

Statistics. Summary data represent means ± SEM (n = 4-6). ANOVA with Bonferroni's post-hoc test or the Mann-Whitney rank sum test was used for the determination of statistical significance among treatment groups, as appropriate. *In vivo*: [a], $p < 0.05$ compared to vehicle; [b], $p < 0.05$ compared to animals exposed LPS alone, [c], $p< 0.05$ compared to animals exposed to CE + LPS.

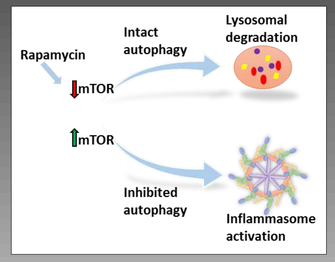

Figure 1: Previous Hypothesis. Increased activation of mTOR inhibits autophagy. Autophagy has been shown to negatively regulate inflammasome activation.[6] However, inhibition of mTOR, restores autophagy, allowing for proper regulation of intracellular processes, including blunted inflammasome activation.

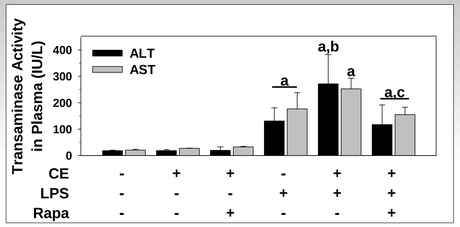

Figure 2: Serum transaminase levels. Mice were treated as described in *Materials and Methods*. Alanine aminotransferase (ALT) and aspartate aminotransferase (AST) were determined in plasma samples collected 48 hours after CE and 24 hours after LPS administration.

Neither CE alone or given with rapamycin altered serum transaminase levels. LPS significantly increased both, ALT and AST levels. CE further enhanced this effect. However, rapamycin significantly blunted transaminase levels.

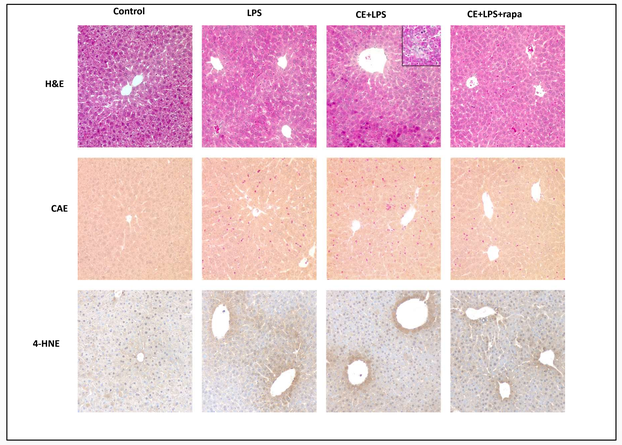

Figure 3: Effect of CE and rapamycin on liver health. Mice were treated and sacrificed as described in *Materials and Methods.* Paraffin-embedded livers were stained with hematoxylin and eosin (H&E) and chloroacetate esterase (CAE) , and 4-hydroxynonenol (4-HNE).

Control samples show no signs of hepatic damage or inflammation. LPS increased necrosis and positive staining for both neutrophil accumulation and oxidative stress. CE further enhanced damage, inflammation, and oxidative stress. Rapamycin blunted necrosis, inflammation, and decreased 4-HNE positive staining.

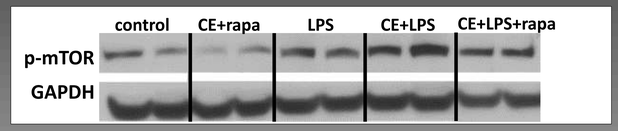

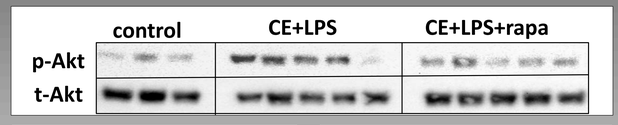

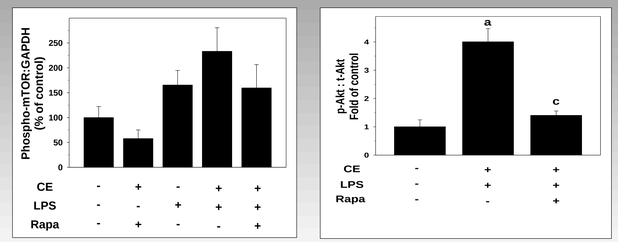

Figure 4: Effect of rapamycin on mTOR activation and Akt inactivation *in vivo*. Mice were treated, hepatic proteins were extracted, and Western Blots were performed as described in *Materials and Methods*.

Preliminary data have shown that CE increases mTOR phosphorylation, suggesting a role for mTOR in CE-induced liver injury.[6] Here, CE further enhanced mTOR activation, however, rapamycin blunted mTOR activation, not only after CE+ LPS but also after CE alone. CE+LPS enhanced Akt activation while rapamycin blunted the impact.

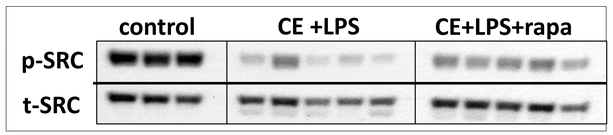

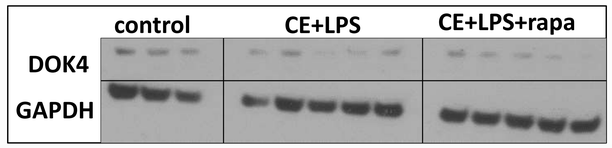

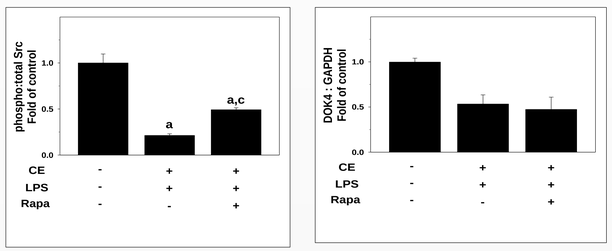

Figure 5: Effect of rapamycin on Src activation and Dok4 *in vivo*. Mice were treated, hepatic proteins were extracted, and Western Blots were performed as described in *Materials and Methods*.

Here, CE+LPS inactivated Src phosphorylation, however, rapamycin blunted Src inactivation. No significant difference was detected between CE+LPS and CE+LPS+Rapamycin in DOK4 activation.

SUMMARY

Rapamycin

- decreases liver damage caused by CE + LPS
- decreases inflammation caused by CE + LPS
- decreases the expression of AKT
- increases the activation of Src
- lowers oxidative stress

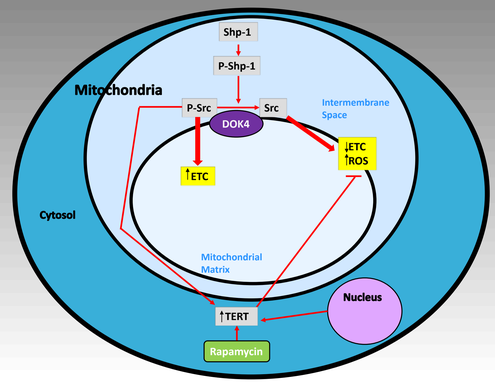

Figure 6: Current Hypothesis.
We have demonstrated previously that VC and its metabolites cause mitochondrial dysfunction; however, the mechanism(s) by which this occurs was previously unclear. Here we hypothesized that VC metabolite exposure dephosphorylates and inactivates Src, which is located at the inner mitochondrial membrane (IM). IM-bound DOK4 is known to facilitate Src dephosphorylation[7]. Inactive Src uncouples the electron transport chain (ETC)[7], thereby increasing the formation of Reactive Oxygen Species (ROS). Expression and mitochondrial localization of TERT is known to be increased by rapamycin, which works to protect against Src inactivation and its impact on ETC and ROS production[8]. The current hypothesis was, therefore that rapamycin is protective in this model by increasing TERT shuttling to the mitochondria and therefore maintaining ETC and decreasing ROS release. The current data supports this hypothesis.

Future Aim

- Further investigation into the Src and Shp-2 pathway
- Further analysis into the translocation of TERT from the nucleus to the mitochondria

REFERENCES

1. Cave,M., Deaciuc,I., Mendez,C., Song,Z., Joshi-Barve,S., Barve,S. & McClain,C. Nonalcoholic fatty liver disease: predisposing factors and the role of nutrition. *J. Nutr. Biochem.* 18, 184-195 (2007).
2. Cave M et al., Toxicant associated steatohepatitis in vinyl chloride workers. Hepatology. 51:474-81 (2010).
3. Day,C.P. & James,O.F. Steatohepatitis: a tale of two "hits"? *Gastroenterology.* 114, 842-845 (1998).
4. Wang,X., Wang,S., Liu,Y., et al. The Hsp90 inhibitor SNX-2112 induces apoptosis of human hepatocellular carcinoma cells: The role of ER stress. *Biochemical and Biophysical Research Communications.* 446, 160-166 (2014).
5. Mohammad MK, Avila D, Zhang J, Barve S, Arteel G, McClain C, Joshi-Barve S. Acrolein cytotoxicity in hepatocytes involves endoplasmic reticulum stress, mitochondrial dysfunction and oxidative stress. *Toxicol Appl Pharmacol.* 265:73-82 (2012).
6. Anders LC, Lang AL, Anwar-Mohamed A, Douglas AN, Bushau AM, Falkner KC, Hill BG, Warner NL, Arteel GE, Cave M, McClain CJ, Beier JI. Vinyl chloride metabolites potentiate inflammatory liver injury caused by LPS in mice. *Toxicological Sciences* 2016; in press.
7. Sanda Win, Tin Aung Than, Robert Win Maw Min, Mariam Aghajan, Neil Kaplowitz. c-Jun N-terminal kinase mediates mouse liver injury through a novel Sab (SH3BP5)-dependent pathway leading to inactivation of intramitochondrial Src. Hepatology, VOL. 63, NO. 6, 2016.
8. Judith Haendeler, Stefan Dröse, Nicole Büchner, Sascha Jakob, Joachim Altschmied, Christine Goy, Ioakim Spyridopoulos, Andreas M. Zeiher, Ulrich Brandt, Stefanie Dimmeler. Mitochondrial Telomerase Reverse Transcriptase Binds to and Protects Mitochondrial DNA and Function From Damage.

FUNDING SUPPORT

This research was supported by National Cancer Institute grant R25- CA134283, NIDDK (JIB; CJM), NIEHS (MC), NIAAA (CJM), and the Veterans Administration (MC, CJM).

Genotypic Analysis of *Mammary Carcinoma Susceptibility 3* Nominated Gene Expression Levels in Rat Mammary Glands

Sarah McQuaide, Emily Duderstadt, and David J. Samuelson
Department Biochemistry and Molecular Genetics, University of Louisville School of Medicine

Abstract

In previous studies, it has been concluded that mammary cancer susceptibility in rats is strongly influenced by the *Mammary carcinoma susceptibility 3* quantitative trait locus (*Mcs3* QTL). This was tested using the cancer susceptible Wistar Furth (WF) strain and the cancer resistant Copenhagen (Cop) strain in congenic studies. Exploration into this topic, using WF.Cop congenic strains, narrowed the *Mcs3* QTL region, and provided framework for further genetic testing of genes that reside in the *Mcs3* region. Mammary gland transcript levels of select *Mcs3* nominated genes, *Ilk, Pak1, Rsf1*, and *Il18bp*, were measured in order to determine if there were differences between Cop and WF strains or environment. It was our hypothesis that there is significant difference in the expression of these genes between these two strains. Rat *Ilk, Pak1, Rsf1,* and *Il18bp* expression was measured using Taqman quantitative PCR. The *Mcs3* nominated genes in this study were chosen because they have been shown to potentially have a role in breast cancer. Rat *Rplp2* was used as an endogenous control gene. Rat *Ilk, Rsf1,* and *Il18bp* expression was not significantly different between Copenhagen or Wistar Furth strains or in those that received DMBA vs those that did not. Rat *Pak1,* however, had different expression depending on environmental exposure to DMBA. An effect of genotype on rat *Pak1* was not detected. Another published study established a positive relationship between the expression of mouse *Pak1* and mammary cancer susceptibility. The results of our study confirms this relationship, and suggests that endogenous expression of rat *Pak1* is increased following exposure to DMBA, a mammary carcinogen; therefore, suggesting that environmental exposures may influence *PAK1* expression phenotype more than genotype. These findings have important relevance to female breast cancer as they suggest environmental expression is important to *Pak1* expression.

Introduction

- Wistar Furth (WF) rats demonstrate a mammary cancer susceptible phenotype while Copenhagen (Cop) demonstrates a resistant phenotype.
- Previously, our lab conducted WF.Cop congenic rat studies to narrow the *Mammary cancer susceptibility 3* quantitative trait locus (*Mcs3* QTL).
- Using information from our lab's congenic studies, we selected four *Mcs3*-nominated candidate genes, rat *Ilk, Pak1, Rsf1*, and *Il18bp*, from 310 possible annotated genes to test for differences in expression between Cop and WF strains.

Hypothesis

- We hypothesize one or more *Mcs3*-nominated gene transcripts are differentially regulated between susceptible Wistar Furth and resistant Copenhagen rat strains.

Results

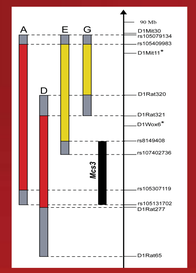

1

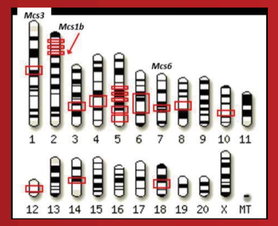

2

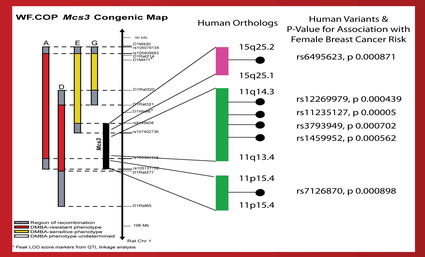

3

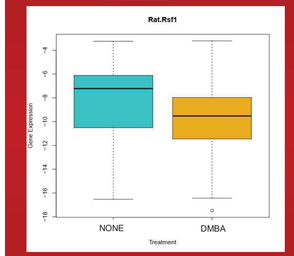

4

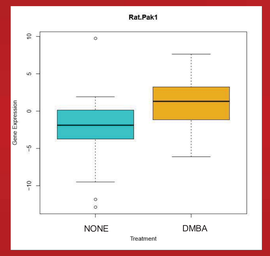

5

gene	Effect of Line P-value	Effect of Treatment P-value	Interaction P-value
Rat.Ilk	0.728098	0.472312	0.718203
Rat.Rsf1	0.479625	0.105448	0.555352
Rat.Il18bp	0.383969	0.820746	0.105363
Rat.Pak1	0.189851	0.020877	0.554196

6

Figure 6: P-values from 2-way ANOVA; Note that p≤ 0.05 for rat *Pak1*

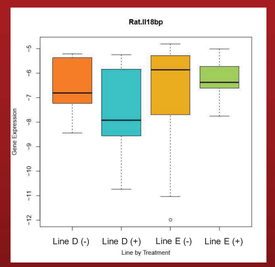

7

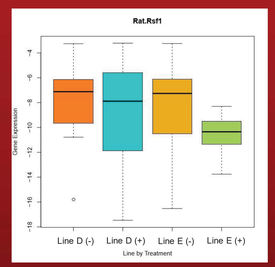

8

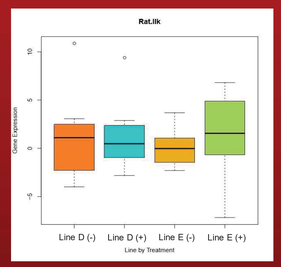

9

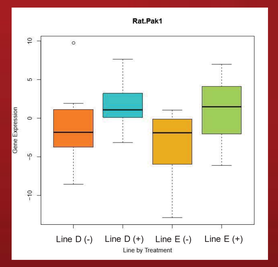

10

Figure 1 depicts the congenic map of the *Mcs3* QTL
Figure 2 is an ideogram of showing the location of known rat mammary carcinoma susceptibility QTLs.
Figure 3 is a map depicting human orthology in relation to the *Mcs3* QTL.
Figures 4 and 5 depict results of expression vs. treatment for rat *Rsf1* and *Pak1*
Figures 7 - 10 are box and whisker plots for each gene with results by congenic strain and environmental exposure plotted.

Methods

- We selected four Mcs3 nominated genes (rat *Ilk, Pak1, Rsf1, and Il18bp*) that have known associations with breast cancer.
- Inguinal mammary tissue was harvested from Wistar Furth (WF) and Copenhagen (Cop) rat congenic strains (WF.Cop) with or without exposure to 7,12-Dimethylbenz[a]anthracene (DMBA).
- Tissues were homogenized in Tri-reagent for RNA extraction. RNA samples with 260/230 ratios less than 1.2 were not used.
- This left 46 samples from 46 rats (WF rats with DMBA = 12; WF rats without DMBA = 13; WF.Cop without DMBA = 10; WF.Cop with DMBA = 11).
- cDNA was made from the extracted RNA using SuperScript II, a reverse transcriptase, and re-suspended in DEPC water.
- 5' FAM labeled Taqman probes for rat *Ilk, Pak1, Rsf1, Il18bp,* and *Rplp2* were mixed with the diluted cDNA for qPCR. Each sample had three replicates.
- Absolute quantification was used to measure transcript levels.
- Standard curves were based on pooled cDNA from eight WF rats without DMBA.
- The average sample quantity was divided by its corresponding Rplp2 quantity and converted to $\log_2$.
- This resulting quantity was used in a 2-way ANOVA to test for effects of *Mcs3* genotype and environmental exposure (DMBA).

Conclusion

- Our results suggest that environmental exposure of DMBA had an effect on *Pak1* expression, suggesting that expression phenotype is linked more to environmental exposure than to genotype.
- *Pak1* was expressed more in rats that received DMBA.
- The results of this experiment suggest that there is no difference in expression of rat *Ilk, Rsf1,* and *Il18bp* regardless of treatment or strain.

Future Directions

- Other genes within the *Mcs3* QTL should be explored to determine if they follow a similar pattern or if there is a genotypic effect on expression.
- Expression of *Mcs3* nominated genes should also be tested in other rat tissues (i.e. ovaries).

Acknowledgments

- Funding by the R25-CA 134283 grant from the National Cancer Institute and the Department of Biochemistry and Molecular Genetics, University of Louisville School of Medicine
- Dr. Corey Watson for his assistance in statistical analysis

Analysis of Organ and Cell-Specific Gene Manipulation With Nanoparticles

Brandon Nguyen-Ho, Lauren G. Poole[1,2], Kimberly Head[1], Juliane Beier[1,2] Jill Steinbeck[1] and Gavin E. Arteel[1,2]

[1] Department of Pharmacology and Toxicology, [2] University of Louisville Alcohol Research Center, University of Louisville Health Sciences Center, Louisville KY 40292, USA

ABSTRACT

Background. Several studies indicate substantial interdependence between liver and lung cancers. Lung cancer is metastatic to other regions of the body, but generally spreads to the liver. A liver specific knockout model has been established, where intrasplenic injections of tamoxifen-loaded Poly(lactic-co-glycolic acid) (PLGA) nanoparticles activate a site specific Cre recombinase to excise the loxP flanked gene of interest, the red fluorescence, within Kupffer cells. This leaves the Kupffer cells to express green fluorescence. The collected hepatic cell populations are prepared and fixed to analyze through flow cytometry.

Objective. The goal of the study was to determine the percentages of Kupffer cells and other hepatic cell subsets that express green fluorescence, due to the tamoxifen inducible Cre-mediated excision of the red fluorescence.

Methods. Six month old R26CreER/mTmG mice received intrasplenic injections with either saline or tamoxifen-loaded PLGA nanoparticles (0.75 mg / 25 g body weight in 200 µL sterile saline). Mice behavior and health were monitored for one week post-surgery and sacrificed 15 days post-surgery. The perfused liver samples were collected for analysis by flow cytometry.

Results. Our flow cytometry data suggests a poor detection of green fluorescence in the collected liver samples. The intrasplenic injection of tamoxifen-loaded nanoparticles showed only a 2.50%, 3.11%, 8.86%, and 18.4% expression of the green fluorescence in Kupffer cells, LSEC, Stellate cells, and Hepatocytes respectively.

Conclusions. We expected to see a intrasplenic tamoxifen-loaded nanoparticle GFP expression similar to, if not greater than, the I.P tamoxifen expression of GFP. The poor detection of green fluorescence in the collected liver samples may be attributed to the differing times of sacrifice, low dosages of tamoxifen-loaded nanoparticles, the significant amount of dead cells post-sacrifice, and inappropriate compensation control. In the future, this study will seek to correct these variables through optimizations of the experiment which include: sacrificing the mice in a timely manner post-injection, examining mice injected at greater doses of tamoxifen-loaded nanoparticles, improving the liver perfusion digest protocol for specific hepatic subsets, and creating appropriate compensation control.

BACKGROUND

Kupffer cells are specialized macrophages located in the liver and constitute the largest resident macrophage population in the body. These cells are also a major source for systemic levels of cytokines and chemokines. Previous studies by this group has suggested that Kupffer cell-derived tumor necrosis factor alpha (TNFα) is a key cytokine involved in a liver-lung axis, which may mediate pulmonary inflammation.[1] Such an axis may well also contribute to pulmonary carcinogenesis and represent an exciting new 'druggable target.'

Definitive experimental proof of this axis has been limited, as there is currently no viable technique to selectively alter the Kupffer cells without transducing other macrophage populations, including those of the lungs. There are several techniques that purportedly selectively transduce Kupffer cells, but these approaches all lack true specificity for this cell type. For example, 'Kupffer cell chimeras' can be created in which the host Kupffer cells are repopulated with transduced bone marrow cells; however, the methods to remove the native cell population (e.g., liposomal chlodronate), also target other macrophage populations. Likewise, transgenic approaches that target macrophages (e.g., LysM-driven expression) are not specific for Kupffer cells.[2] Viral vectors (e.g., rAd and rAAV) suffer from either low transduction efficiency or transient transduction. The goals of the current work are to overcome these limitations.

In this study, locational and temporal control of Cre was employed to attempt to make conditional 'Kupffer cell knockouts.' This model consists of a site-specific recombinase (Cre) that allows insertions, deletions, inversions and translocations at targeted (i.e., "floxed") sites of DNA within the cell (Figure 3). Locational control of Cre expression was attempted by administration of the chemical inducer of Cre expression (tamoxifen), encapsulated in PLGA nanoparticles. These nanoparticles are robustly engulfed by Kupffer cells.[3] To facilitate specificity to hepatic macrophages, nanoparticles were injected intrasplenically. Previous work by this group supports the hypothesis that this approach does indeed selectively transduce hepatic cells (Figures 1 and 2). The purpose of this current study was to develop a flow cytometry approach to quantitatively document these changes to the liver.

MATERIALS AND METHODS

Generation of Transgenic Mice: Male mice homozygous for a two-color fluorescent Cre reporter allele (B6.129(Cg)-Gt(ROSA)26Sor$^{tm4(ACTB-tdTomato,-EGFP)Luo}$/J, or simply ROSA$^{mT/mG}$) were purchased from the Jackson Laboratory (Bar Harbor, ME). Upon Cre-mediated recombination, the tdTomato cassette, which is flanked by lox-p sites, is excised, allowing for the expression of the membrane-targeted enhanced green fluorescent protein (EGFP).

Mice and Treatment: Six month old male mice received intrasplenic injections with either saline or tamoxifen-loaded Poly(lactic-co-glycolic acid) (PLGA) nanoparticles. The abdominal hairs of the mice were removed with a razor and then the mice were anesthetized with isoflurane. The spleen was injected with tamoxifen-loaded PLGA nanoparticles with a 28-gauge insulin syringe at a dose of 0.75 mg per 25 g of body weight in 200 µL of sterile saline. A 3-0 silk suture was used to seal the surgical incision. Prior to the procedure, the PLGA nanoparticles were placed in a water bath sonicator for about 75 seconds to separate clumps of nanoparticles. Each mouse was singly housed and sacrificed 15 days after the procedure.

Mice Sacrifice and Liver Perfusion: Mice were anesthetized with a ketamine / xylazine mixture (100/15 mg) using a 28-gauge insulin syringe at a dose of four times the weight of the mouse. The liver was visualized. The liver was perfused with perfusion buffer for six minutes (5 ml/min) and then dissociation buffer for 10 minutes (5 ml/min). The liver was removed and then placed into a petri dish containing preservation buffer. The perfused liver was teased apart until a cloudy mixture was identified and then it was transferred to an iced 50 mL tube for further analysis.

Flow Cytometry: The mice were sacrificed 15 days after the intrasplenic injection of saline or tamoxifen-loaded PLGA nanoparticles. Perfused livers were obtained and the hepatic cells experienced individual intracellular antibody staining with Anti-LRP1 Alexa Fluor 647 (Abcam), CD68 Rat Anti-Mouse BV421 (BD Biosciences), CD31 (PECAM-1) PE-Cyanine7 (eBioscience), and GFAP (GA-5) eFluor 660 (eBioscience). After staining, the cells were fixed in Intracellular Fixation Solution (eBioscience) and Flow Cytometry Staining Buffer (eBioscience). It was stored at 4° C overnight. The samples were taken up to the LSRFortessa Flow Cytometer the next day for further analysis.

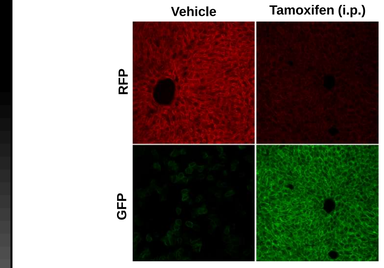

Poole, Liver-Lung Axis, 5:96-97

Figure 1: Intraperitoneal (I.P) administration of tamoxifen successfully induces the Cre-mediated excision of the red fluorescence, leaving the expression of the green fluorescent protein.

Studies in our lab have shown that an I.P injection of tamoxifen successfully cleaved the flox flanked tdTomato (RFP) cassette, leaving only the green fluorescent protein (GFP) expression visible in the liver tissue.

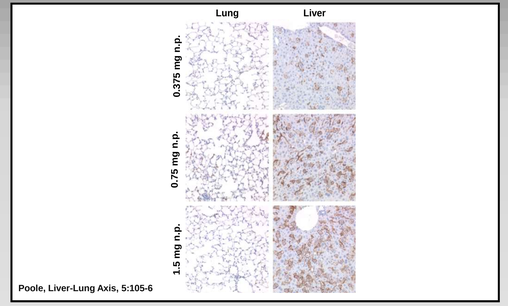

Poole, Liver-Lung Axis, 5:105-6

Figure 2: Membrane targeted GFP expression in the liver and lung after intrasplenic administration of tamoxifen-loaded PLGA nanoparticles.

Studies in our lab have shown that there was no observable increase in GFP staining as the dosage of tamoxifen-loaded nanoparticles increased for the lung. There was little to no GFP staining in the lung because the intrasplenic administration of tamoxifen-loaded nanoparticles primarily induces hepatic circulation. There was a dose-dependent increase in GFP staining as the dosage of tamoxifen-loaded nanoparticles increased for the liver. This confirms that the intrasplenic injection is successful in providing GFP expression overwhelmingly in the liver.

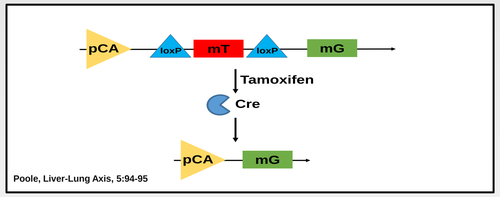

Poole, Liver-Lung Axis, 5:94-95

Figure 3: Scheme of tamoxifen-inducible Cre-mediated excision of the mT/mG construct.

The mice have a native two-color fluorescent Cre reporter allele mentioned in the Materials and Methods. Tamoxifen is the chemical inducer of the bacterial enzyme Cre. The Cre proceeds to cleave the gene of interest flanked by loxP sites, the red fluorescence (mT). As a result, only the green fluorescent protein is expressed. An intrasplenic administration of tamoxifen-loaded nanoparticles using this scheme allows for Kupffer cell specificity.

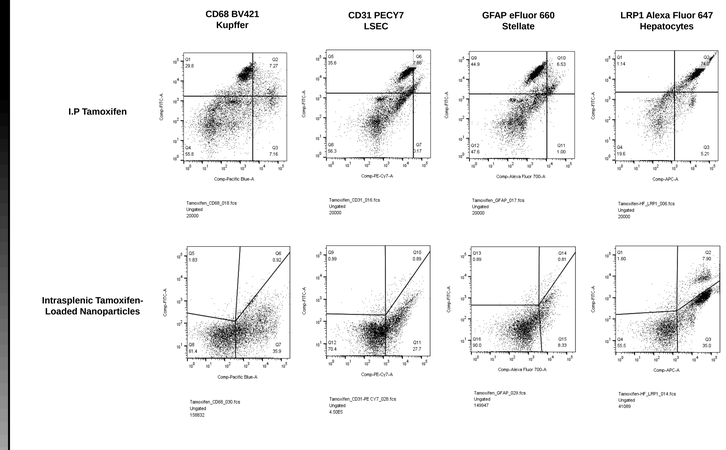

Figure 4: Sample Preparation & Flow Cytometry.

Samples were individually stained with antibodies corresponding to the specific hepatic cell subsets. It was fixed at 4° C overnight. The LSRFortessa Flow Cytometer collected data from the samples and FlowJo v10 was used to create the graphs shown in Figure 4. The graphs are organized to display I.P tamoxifen administration versus intrasplenic tamoxifen-loaded nanoparticle administration for each hepatic cell subset.

I.P Tamoxifen Administration	% GFP+ In Antibody Positive Events	Intrasplenic Tamoxifen Administration	% GFP+ In Antibody Positive Events
Kupffer Cells	50.4 %	Kupffer Cells	2.50 %
LSEC	97.9 %	LSEC	3.11 %
Stellate Cells	86.7 %	Stellate Cells	8.86 %
Hepatocytes	93.4 %	Hepatocytes	18.4 %

Table 1: Analysis and Comparison of Positive GFP Expression Results, I.P Administration versus Intrasplenic Administration.

The following table documents the percentages of green fluorescent protein (GFP) expressing cells for intraperitoneal tamoxifen administration versus intrasplenic tamoxifen-loaded PLGA nanoparticle administration. It was calculated by: (% Double Positive Cells in Top Right Quadrant)/(Total % Events in Top Right and Bottom Right Quadrants) X 100. The percent expression of GFP for the I.P tamoxifen injection was greater than the intrasplenic tamoxifen-loaded nanoparticle injection for all hepatic populations. We were hoping to see a similar, if not greater, expression of GFP within the Kupffer cells for the intrasplenic injection. There are several factors that might have contributed to these results. The I.P mice were observed 8 days post-injection while the intrasplenic mice were observed 15 days post-injection. Previous studies in our lab (Figure 1 and 2) have only observed the liver at 7 days post-injection which may raise concerns about possible turnover within the cells as time progresses. Also, the administration technique and amount of tamoxifen and tamoxifen-loaded nanoparticles injected varied between these two groups; the I.P group received 0.075 mg tamoxifen / g body weight for three consecutive days while the intrasplenic group received 0.75 mg / 25 g of body weight for a single day. Other factors that might have contributed to these results include the significant amount of dead cells viewed under the microscope, the lack of additional antibody surface markers for cell differentiation and specificity, inappropriate compensation control, and large amounts of autofluorescence within the cells.

Figure 5: Experimental Procedure.

Male mice homozygous for a two-color fluorescent Cre reporter allele B6.129(Cg)-Gt(ROSA)26Sor$^{tm4(ACTB-tdTomato,-EGFP)Luo}$/J were injected intrasplenically with saline or tamoxifen-loaded nanoparticles. The mice were sacrificed 15 days post-injection and the perfused liver samples were collected. The liver samples were stained and fixed at 4° C overnight. Flow cytometry analysis was performed the following day.

SUMMARY

1. Intrasplenic administration of tamoxifen-loaded PLGA nanoparticles is performed rather than I.P because intrasplenic administration primarily induces hepatic circulation, instead of systemic.
2. The intrasplenic administration of tamoxifen-loaded PLGA nanoparticles, in principle, will selectively cleave the red fluorescence and leave only the green fluorescence expression within the Kupffer cells.
3. The percentages of GFP expression for the intrasplenically injected mice were unexpected and may be due to several factors described under Table 1.

FUTURE DIRECTION

Future work will focus on optimizing the protocol and parameters of this study.

1. Sacrifices should be performed at or very near 7 days post-injection.
2. The liver perfusion digest protocol must be optimized to a specific hepatic cell subset. This will substantially reduce the number of dead cells in the digest. Live and dead cells must be discriminated because dead cells can nonspecifically bind to different antibodies, likely yielding inaccurate results.
3. Mice injected at greater doses of tamoxifen-loaded nanoparticles will be examined. Figure 2 demonstrates that increasing doses of tamoxifen-loaded nanoparticles will increase GFP expression in the liver.
4. Additional antibodies, including surface markers, must be added to properly obtain cell specificity and differentiation.
5. An appropriate control for GFP and tdTomato must be found for the correct application of compensation control.

REFERENCES

1. Massey V, et al, Chronic alcohol exposures enhances lipopolysaccharide-induced lung injury in mice. Alcohol Clin Exp Res. 2015 October;39(10):1978-1988. doi: 10.1111/acer.12855.

2. Poole L, Novel Insight Into The Liver-Lung Axis In Alcohol-Enhanced Acute Lung Injury. 2016:5: 89-113.

3. Park J-K, et al, Cellular distribution of injected PLGA-nanoparticles in the liver. Nanomedicine: NBM 2016:12:1365-1374.

FUNDING SUPPORT

This research was supported by the NIH/NCI (R25-CA134283) and NIH/NIAAA (1R01AA021978-01) and are gratefully acknowledged.

Strain Differences in Susceptibility to Cisplatin-Induced Renal Fibrosis

Gabrielle Oropilla[1], Cierra Sharp[1], Mark Doll[1], Leah Siskind[1,2]
[1]Department of Pharmacology & Toxicology, University of Louisville, Louisville, KY
[2]James Graham Brown Cancer Center, Louisville, KY

Introduction

- Cisplatin is a potent chemotherapeutic used to treat a multitude of solid cancers.
- The dose-limiting side effect of this drug is nephrotoxicity, causing acute kidney injury (AKI) in 30% of adult patients.
- Patients with cisplatin-induced AKI are more likely to develop end stage renal diseases, particularly chronic kidney disease (CKD), which is marked by the development of fibrosis.
- Currently, there are no therapeutic interventions for cisplatin-induced kidney injury, which may be due to limitations in the current mouse model used to study this type of injury.

Standard Model

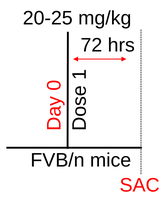

Repeated Dosing Model

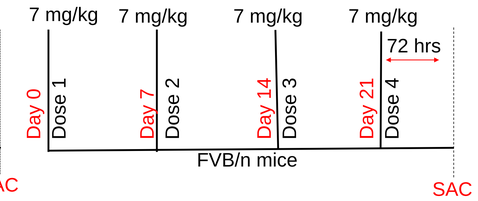

Rationale for this Study

- C57BL/6J mice is a strain frequently used in renal studies.
- This strain is resistant to some forms of renal fibrosis, such as glomerular fibrosis.

Myofibroblast Detection by αSMA IHC

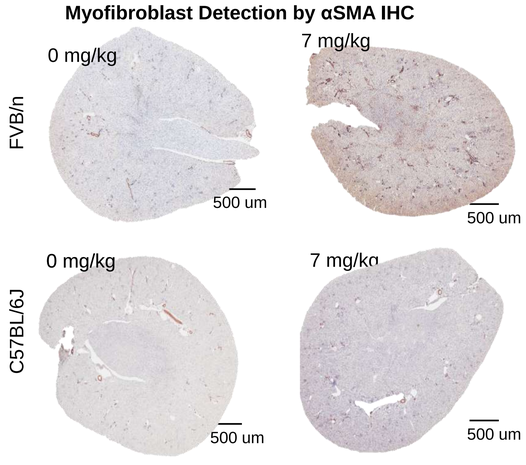

Total Collagen Deposition by Sirius Red/ Fast Green Staining

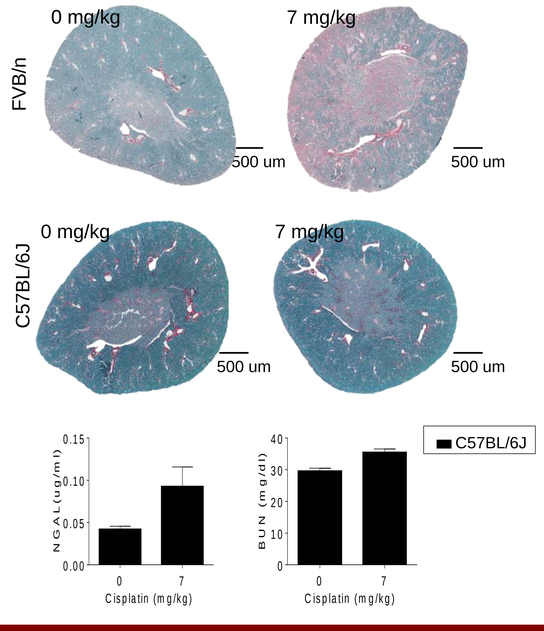

Hypothesis

- C57BL/6J mice, a strain commonly used in renal studies that is resistant to some forms of fibrosis, will require a higher dose of cisplatin in order to develop interstitial fibrosis that occurs with repeated dosing of cisplatin.

Methods

- Five male C57BL/6J mice were treated with vehicle saline once a week for four weeks and ten male C57BL/6J mice (8 weeks old) were treated with 9 mg/kg of cisplatin once a week for four weeks; both groups were sacrificed three days after the last injection. The same protocol was conducted with FVB/n mice but treated with 7 mg/kg of cisplatin.
- QRTPCR, IHC, and Western blot analysis were utilized to determine the presence of fibrosis in these mice, as well as compare fibrotic and inflammatory markers to FVB/n mice treated with cisplatin.

Repeated Dosing Regimen

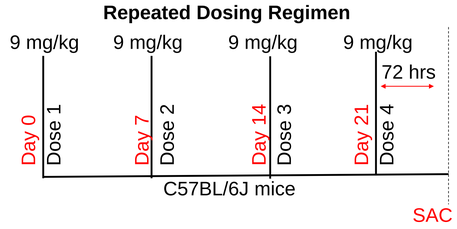

Results

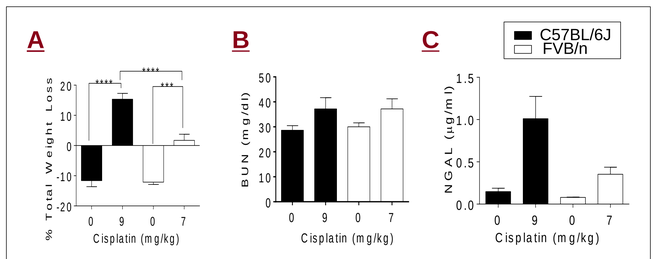

Figure 1: % Total Weight, BUN, NGAL. **(A)** Percent total weight loss at Day 24, **(B)** Blood, urea, nitrogen (BUN) as a measure of kidney function, and **(C)** Neutrophil gelatinase associated lipocalin (NGAL), a kidney injury marker measured in urine.

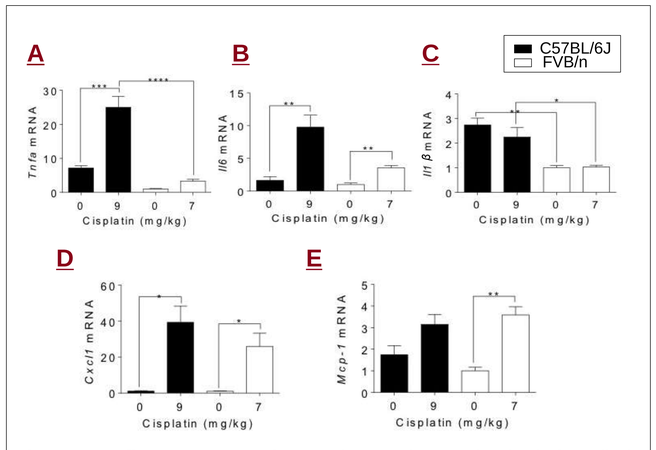

Figure 2: Inflammatory Markers. Injury to the proximal tubule cells in the cortex leads to inflammation. **(A)** Tnfα is a mediator of inflammatory tissue damage, **(B)** Il6 promotes maintenance of a chronic inflammatory state, **(C)** Il1β is a mediator of inflammation as well as cell proliferation, differentiation, and apoptosis, **(D)** Cxcl1 recruits neutrophils to sites of tissue inflammation, and **(E)** Mcp-1 plays a role in macrophage recruitment and activation.

Results

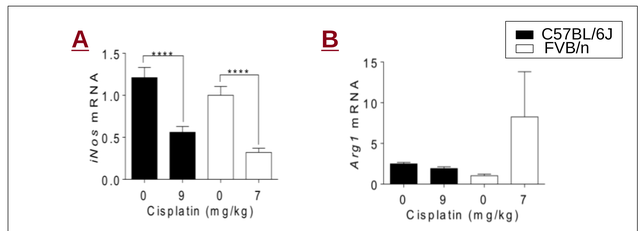

Figure 3: Macrophage Types. Macrophages play a major role in renal repair post injury. **(A)** iNos is a M1 pro-inflammatory macrophage, characteristic of maladaptive repair. **(B)** Arg1 is a M2 anti-inflammatory macrophage, characteristic of adaptive repair.

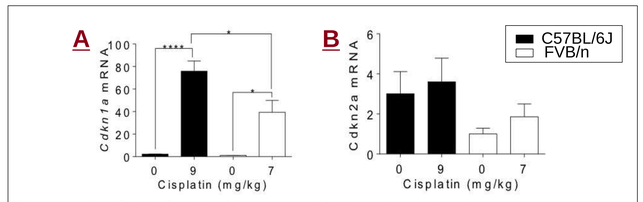

Figure 4: Cell Cycle Markers. Cell cycle activation and inhibition regulates DNA repair. **(A)** Cdkn1a is a regulator of cell cycle progression at the G1 phase. **(B)** Cdkn2a regulates cell growth and division by decelerating cell progression from the G1 to S phase.

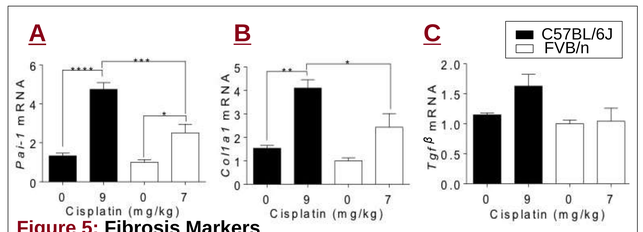

Figure 5: Fibrosis Markers
(A) Pai-1 is produced by inflammatory cells and leads to the accumulation of scar tissue in the kidney. **(B)** Col1a1 encodes for collagen type 1 protein. **(C)** Tgfβ activates pathways that increase extracellular matrix protein deposition, particularly fibronectin.

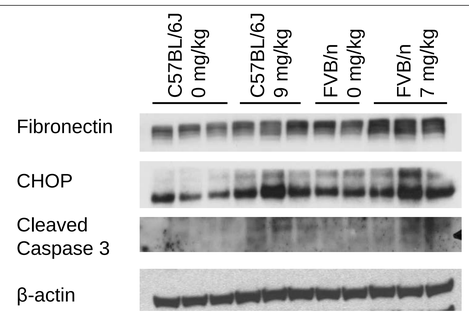

Figure 6: Markers of Fibrosis, ER Stress, and Apoptosis. Fibronectin is a marker of fibrosis, CHOP of endoplasmic reticulum stress, and Cleaved Caspase 3 of apoptosis. β-actin was the control.

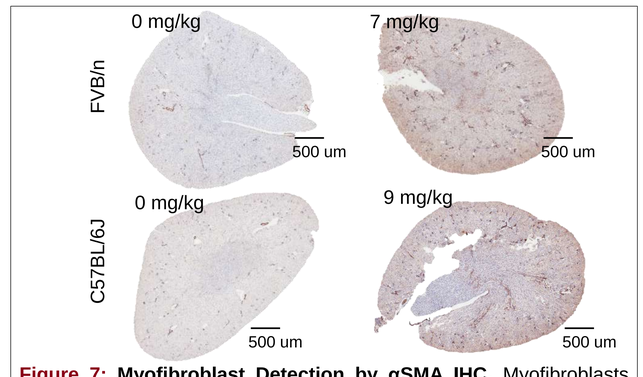

Figure 7: Myofibroblast Detection by αSMA IHC. Myofibroblasts produce extracellular matrix and are expressed to repair and restore homeostasis after injury.

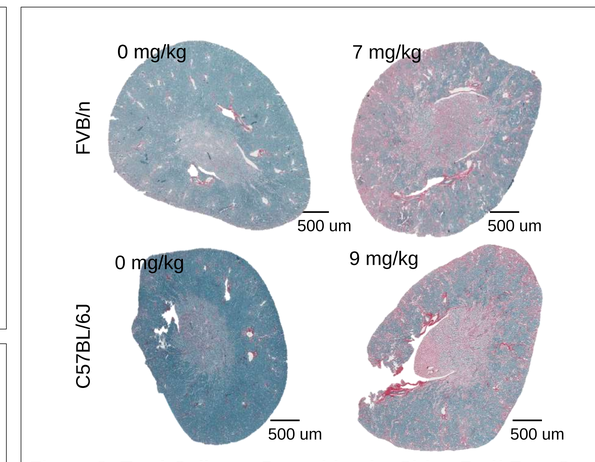

Figure 8: Total Collagen Deposition by Sirius Red/ Fast Green Staining. Extracellular matrix production results in collagen buildup.

Clinical Impact

- Human patients diagnosed with cancer are administered low doses of cisplatin over an extended period of time in order to limit nephrotoxicity while maintaining therapeutic efficacy.
- Genetic factors may play a role in human fibrosis. By studying different strains of mice, we will better understand whether genetic susceptibility plays a role in fibrogenesis.
- This information could be translated to the differential effects of cisplatin in humans and susceptibility to drug toxicities in order to determine a patient's optimal administration and dosage.

Conclusions

- C57BL/6J mice are susceptible to developing renal fibrosis when treated with 9 mg/kg cisplatin once a week for 4 weeks.
- Strain differences indicate that C57BL/6J mice need a higher dose of cisplatin in order to develop fibrosis in comparison to FVB/n mice.

Future Directions

- Current studies are underway for FVB/n mice treated with 9 mg/kg cisplatin once a week for 4 weeks.
- Repeat the repeated dosing regimen in other strains of mice in order to fully study genetic variability.

Acknowledgments

- This research was supported by the NIH: National Cancer Institute Grant R25-CA134283.

References

1. Sharp *et al.* "Repeated Administration of Low-Dose Cisplatin in Mice induces Fibrosis." *American Journal of Physiology- Renal Physiology* 2016 310:6.
2. Walkin *et al.* "The Role of Mouse Strain Differences in the Susceptibility to Fibrosis: A Systematic Review." *Fibrogenesis & Tissue Repair* 2013 6:18.